Colloids and Surfaces B: Biointerfaces 161 (2018) 365–374

Contents lists available at ScienceDirect

Colloids and Surfaces B: Biointerfaces

journal homepage: www.elsevier.com/locate/colsurfb

Full length article

Size-dependent effect of cystine/citric acid-capped confeito-like gold nanoparticles on cellular uptake and photothermal cancer therapy

Wen Shang Saw[a], Masaki Ujihara[b], Wu Yi Chong[c], Siew Hui Voon[a], Toyoko Imae[b,d,**], Lik Voon Kiew[e], Hong Boon Lee[a], Kae Shin Sim[f], Lip Yong Chung[a,*]

[a] Department of Pharmacy, Faculty of Medicine, University of Malaya, 50603 Kuala Lumpur, Malaysia
[b] Graduate Institute of Applied Science and Technology, National Taiwan University of Science and Technology, 43 Section 4, Keelung Road, Taipei 10607, Taiwan
[c] Photonics Research Centre, Faculty of Science, University of Malaya, 50603 Kuala Lumpur, Malaysia
[d] Department of Chemical Engineering, National Taiwan University of Science and Technology, 43 Section 4, Keelung Road, Taipei 10607, Taiwan
[e] Department of Pharmacology, Faculty of Medicine, University of Malaya, 50603 Kuala Lumpur, Malaysia
[f] Institute of Biological Science, Faculty of Science, University of Malaya, 50603 Kuala Lumpur, Malaysia

ARTICLE INFO

Article history:
Received 16 June 2017
Received in revised form
17 September 2017
Accepted 25 October 2017
Available online 26 October 2017

Keywords:
Gold nanoparticles
Cystine
Size
Endocytosis
Intracellular localization
Photothermal cytotoxicity

ABSTRACT

Physiochemical changes, including size, are known to affect gold nanoparticle cellular internalization and treatment efficacy. Here, we report the effect of four sizes of cystine/citric acid-coated confeito-like gold nanoparticles (confeito-AuNPs) (30, 60, 80 and 100 nm) on cellular uptake, intracellular localization and photothermal anticancer treatment efficiency in MDA-MB231 breast cancer cells. Cellular uptake is size dependent with the smallest size of confeito-AuNPs (30 nm) having the highest cellular internalization via clathrin- and caveolae-mediated endocytosis. However, the other three sizes (60, 80 and 100 nm) utilize clathrin-mediated endocytosis for cellular uptake. The intracellular localization of confeito-AuNPs is related to their endocytosis mechanism, where all sizes of confeito-AuNPs were localized highly in the lysosome and mitochondria, while confeito-AuNPs (30 nm) gave the highest localization in the endoplasmic reticulum. Similarly, a size-dependent trend was also observed in *in vitro* photothermal treatment experiments, with the smallest confeito-AuNPs (30 nm) giving the highest cell killing rate, whereas the largest size of confeito-AuNPs (100 nm) displayed the lowest photothermal efficacy. Its desirable physicochemical characteristics, biocompatible nature and better photothermal efficacy will form the basis for further development of multifunctional confeito-AuNP-based nanotherapeutic applications.

1. Introduction

Gold nanoparticles (AuNPs) have attracted both scientific and technological interest due to their inert nature, chemical stability and ease of synthesis. As a result, there have been many studies on the applications of AuNPs in biological imaging and drug delivery in the past decade [1]. Furthermore, the unique optical property of AuNPs to absorb and convert photon energy into thermal energy based on localized surface plasmon resonance renders them useful for photothermal cancer therapy [2]. Huang et al. [3] demonstrated the capability of rod shaped-AuNPs to cause photodestruction after internalization into cancer cells. The uptake of nanoparticles by tumor cells is crucial because the cellular uptake ability of AuNPs enables photothermal treatment (PTT) to achieve greater tumor therapeutic specificity with fewer off-target effects [4].

Physiochemical differences in nanoparticles such as particle size affect the uptake efficiency and kinetics, internalization mechanism and intracellular localization [5]. While studies have reported size-dependent internalization efficiency with a greater uptake of smaller sized AuNPs [6,7], some studies have reported that the optimal size for the cellular uptake of AuNPs is 40–50 nm compared with other sizes [8,9]. This optimum size range was suggested to have the fastest membrane wrapping time and receptor-ligand interaction to produce sufficient free energy to drive the NPs into the cell. However, it remains a challenge to establish a general conclusion to correlate the cellular responses to NP size, due to the different physicochemical properties of the particle, cell type, dosing parameters, and measurement methods [10,11].

* Corresponding author at: Department of Pharmacy, Faculty of Medicine, University of Malaya, 50603 Kuala Lumpur, Malaysia.
** Corresponding author.
E-mail addresses: imae@mail.ntust.edu.tw (T. Imae), chungly@hotmail.com (L.Y. Chung).

https://doi.org/10.1016/j.colsurfb.2017.10.064
0927-7765/

Macropinocytosis, and clathrin- and caveolae-mediated endocytosis pathways are important for the cellular uptake of NPs, which are usually coated with plasma proteins when exposed to physiological fluids [12]. Even if they are homologs, AuNPs of different sizes are often internalized into cells through different endocytic mechanisms [13]. The nature of endocytosis potentially dictates the subcellular localization of AuNPs, enabling the possibility to develop AuNP-based drug carriers with subcellular targeting ability [14].

Finally, size affects the ability of AuNPs to convert light to heat energy, influencing the photothermal conversion efficiency. Several studies have investigated the photothermal conversion efficiencies of AuNPs with different sizes. Small gold nanospheres (sphere-AuNPs) of 20 nm exhibited higher photothermal conversion efficiency (97–103%) than gold nanocages of 85 nm (64%) and gold nanoshells of 152 nm (39%) [15–17]. However, some of the variation in these reported values might be due to the differences in the laser irradiation conditions, nanoparticle shape and dose.

To monitor the effect of particle size on the cellular uptake efficiency and PTT efficacy of AuNPs, a series of confeito-like AuNPs with sizes of 30, 60, 80 and 100 nm was synthesized using a versatile and environmental friendly preparation method [18]. The smallest confeito-AuNPs of 30 nm were included in this study because nanoparticles (10–20 nm) rapidly undergo liver clearance upon intravenous administration [19], while the largest confeito-AuNPs of 100 nm were selected because the nanoparticles with a diameter $\geq$ 150 nm are not internalized by non-phagocytic cells [20]. The biocompatibility of NPs is also highly dependent on the NP's surface chemistry [21]. Therefore, cystine was chosen as a co-protective agent for confeito-AuNPs because of its non-toxicity and high cell permeability properties [22].

To improve the rational design of confeito-AuNP-based drug carriers and treatment devices for biomedical applications, this study investigated the impact of the cystine/citric acid-capped confeito-AuNP size on tumor cellular uptake and anticancer PTT efficacy. The cellular uptake profile, including the endocytic mechanism and intracellular localization for each size of confeito-AuNPs, was evaluated to elucidate the potential uptake pathway of confeito-AuNPs by cancer cells. This would provide important information to the advancement of confeito-AuNPs for applications in drug delivery and therapeutics. To determine which size of confeito-AuNPs has the highest PTT efficacy, biocompatibility and photothermal cytotoxicity experiments were also included for confeito-AuNPs at pre- and post-laser irradiation. Herein, we reported the characterization of confeito-AuNPs, demonstrating how different sizes of confeito-AuNPs at non-toxic concentrations enter the cells and exhibit photothermally induced anti-tumor effects.

2. Methods

2.1. Materials and instruments

3-(4,5-Dimethylthiazol-2-yl)-2,5-diphenyl tetrazolium bromide (MTT), phosphate-buffered saline (PBS), gold standard for microwave plasma atomic emission spectroscopy (MP-AES) and filipin III from *Streptomyces filipinensis* were purchased from Sigma-Aldrich Co. (St. Louis, MO, USA). Amiloride hydrochloride, genistein, dynamin inhibitor I dynasore, chlorpromazine hydrochloride, cytochalasin D, nitric acid and hydrochloric acid were purchased from Merck Millipore (Billerica, MA, USA). All the chemicals were of analytical reagent grade.

Ultrapure Milli-Q water with a resistivity of 18.2 MΩ.cm was used throughout the synthesis and measurements. ProLong Diamond Antifade Mountant, ProLong Gold Antifade Mountant with 4′,6-diamidino-2-phenylindole (DAPI), MitoTracker Red FM (M-22425), ER-Tracker Blue-White DPX (E-12353) and LysoTracker Blue DND-22 (L-7525) were purchased from Molecular Probes, Invitrogen (Eugene, OR, USA).

2.2. Synthesis of cystine/citric acid-capped confeito-AuNPs and FITC-labeled cystine/citric acid-capped confeito-AuNPs

Confeito-AuNPs were synthesized according to the protocol reported by Ujihara et al. [18]. Further details are provided in the supplementary material section of this manuscript.

2.3. Characterization of samples

The zeta potential and average hydrodynamic diameter were determined using a zetasizer (Zetasizer Nanoseries, Malvern). Dispersions were prepared by centrifuging confeito-AuNPs at 12,500×*g* for 45 min, resuspending in water, serum-free Dulbecco's Modified Eagle's medium (DMEM) or complete DMEM (supplemented with 10% of fetal bovine serum (FBS)), followed by incubation for 3 h at 37 °C in a 5% CO_2 humidified chamber. Microscopic observation was performed using a field emission scanning electron microscope (FESEM; Hitachi SU8000, Tokyo, Japan) at an acceleration voltage of 15 kV and a transmission electron microscope (TEM, Hitachi H-7000 and HT7700, Tokyo, Japan) at an acceleration voltage of 100 kV.

The confeito-AuNPs were placed in a 96-well plate and were irradiated using a continuous wave diode-pumped solid-state (DPSS) laser (Millenia Prime, Newport Corporation) for 5 min with a laser emission wavelength at 532 nm. The laser intensity was set at 2 W/cm^2 by controlling the laser power and irradiation area. The temperature change of the suspension was monitored using a thermocouple (Type T, Omega Engineering) with the probe positioned at the center of the suspension. All the measurements were carried out at room temperature (26 °C), and the temperature change of the suspension was recorded over the period of laser irradiation using a data logger (HH127, Omega Engineering).

2.4. Cellular uptake of confeito-AuNPs

The amount of confeito-AuNPs taken in by MDA-MB-231 cells was determined by a microwave plasma atomic emission spectrometer (4100 MP-AES, Agilent Technologies). Prior to analyzing the specimens, a series of gold standard solutions (1.25–20.00 ppm) was prepared, and the radiation emission intensity of each solution was measured. The data obtained were used to establish the standard curve. Thereafter, the amount of confeito-AuNPs taken in by MDA-MB-231 cells was determined in ppm from the standard curve and was expressed in μM.

MDA-MB-231 cells were seeded in 6-well plates at a density of 300,000 cells per well and were cultured for 12 h to allow cell adhesion. The cells were then incubated with confeito-AuNPs at 50 μM Au at 4 and 37 °C atmosphere for 2, 5 and 24 h. Cell culture medium was removed, and the cells were washed 3 times with cold PBS to remove free confeito-AuNPs. The cells were detached using 200 μL of trypsin–EDTA solutions and then were transferred to a borosilicate glass tube and were suspended in 1.0 mL of PBS. To digest the cells, 1 mL of aqua regia solution (nitric acid 65%/hydrochloric acid 37%, 1:3 vol ratio) was added and allowed to stand at room temperature for 2 days. After diluting with water to a total sample volume of 15 mL, these samples were then analyzed for the total gold content by MP-AES. The percentage of confeito-AuNP uptake was expressed as the mean value of triplicate readings. The cellular uptake studies for the cells treated with confeito-AuNPs were also performed at 4 °C for 2 h to assess the effects of temperature on the uptake of NPs.

To study the uptake pathways for different sizes of confeito-AuNPs, MDA-MB-231 cells were preincubated with six endocytosis inhibitors, including amiloride hydrochloride (10 μM), genistein (100 μM), dynasore (40 μM), cytochalasin D (1 μM), chlorpromazine (50 μM) and filipin III (4 μM) for 30 min followed by incubation with confeito-AuNPs (50 μM Au equivalent) for 2 h. The cells were washed three times with cold PBS, trypsinized, and harvested, followed by acid digestion as described previously. The Au content of each sample was determined using MP-AES.

2.5. Intracellular localization of FITC-confeito-AuNPs

FITC-confeito-AuNPs were used to determine the intracellular co-localization. The fluorescence emission intensities of FITC-confeito-AuNPs were measured using a fluorescence microplate reader (Infinite M200, Tecan Group) at 524 nm after excitation at 490 nm. The amounts of FITC conjugated to confeito-AuNPs were the same for all the four sizes of FITC-confeito-AuNPs because they provided the same fluorescence emission intensities at the same concentration when evaluated at 5 different concentrations (1, 12.5, 25, 50 and 100 μM Au equivalent), and the fluorescence intensities were proportional to the concentrations. The intracellular localization of FITC-Confeito-AuNPs was determined based on the protocol described by Viswanathan et al. [23]. Further details are provided in the supplementary material section of this manuscript.

2.6. In Vitro *photothermal anticancer therapy*

For the cytotoxicity test without laser treatment, the MDA-MB-231 cell line was grown and maintained in complete DMEM at 37 °C in a 5% CO_2 humidified chamber. MDA-MB-231 cells were seeded in 96-well plates at 10,000 cells/well and were incubated overnight for cell adherence. Confeito-AuNPs diluted in culture medium were added to the cells to give final Au concentrations ranging from 0.1 to 100 μM. The cells were then incubated for 24 h at 37 °C in 5% CO_2. The cell viability was assessed using the MTT assay. Details about the MTT assay procedure are provided in the supplementary material section of this manuscript.

For PTT, MDA-MB-231 cells were treated with different concentrations of confeito-AuNPs followed by incubation for 2 h at 37 °C, 95% humidified atmosphere and 5% CO_2. Thereafter, cells were irradiated with a DPSS laser (532 nm, 2 W/cm^2) for 60 s. After laser treatment, cell viability was assessed using the MTT assay.

2.7. Statistical analysis

All the results were presented as the means ± standard deviation (SD). Statistical significance of the differences between different groups was evaluated by independent T test or analysis of variance (ANOVA) with Tukey's posttest. Differences were considered statistically significant at $p < 0.05$ and $p < 0.01$.

3. Results and discussion

3.1. Characterization of confeito-AuNPs

The average hydrodynamic diameters for confeito-AuNPs of 30, 60, 80 and 100 nm suspended in water were increased to 29.4, 63.8, 81.4 and 104.1 nm, respectively, while the zeta potential ranged narrowly from −34 to −43 mV (Table 1). Meanwhile, the average hydrodynamic diameter of confeito-AuNPs became 6- to 10-fold larger when suspended in serum-free DMEM. This suggests that confeito-AuNPs tended to aggregate in serum-free DMEM, and the stability of confeito-AuNPs was reduced. This tendency was corroborated by the less negative zeta potential in serum-free DMEM. The high ionic strength of serum-free media compressed the electric double layer and reduced the electrostatic repulsion force between confeito-AuNPs, allowing the van der Waals attractive force to dominate and cause aggregation of confeito-AuNPs [24].

Table 1
Physical parameters of confeito-AuNPs in water, serum-free DMEM and complete DMEM. The data are represented as means ± SD, (n = 3).

Sample	Average Hydrodynamic Diameter (nm)	Zeta Potential (mV)
Confeito-AuNP 30 nm		
Water	29.4 ± 0.3	−33.87 ± 1.20
Serum Free DMEM	352.6 ± 20.8	−13.80 ± 0.50
Complete DMEM	37.1 ± 0.5	−10.42 ± 0.61
Confeito-AuNP 60 nm		
Water	63.8 ± 2.6	−35.63 ± 1.66
Serum Free DMEM	550.2 ± 71.6	−18.37 ± 0.87
Complete DMEM	70.1 ± 1.3	−10.82 ± 0.33
Confeito-AuNP 80 nm		
Water	81.4 ± 0.6	−39.8 ± 0.80
Serum Free DMEM	679.2 ± 24.6	−15.40 ± 0.57
Complete DMEM	96.0 ± 1.0	−12.43 ± 1.03
Confeito-AuNP 100 nm		
Water	104.1 ± 0.8	−42.63 ± 0.61
Serum Free DMEM	663.8 ± 26.0	−20.20 ± 0.08
Complete DMEM	112.6 ± 0.8	−11.37 ± 1.12

Table 2
Number of tips per confeito-AuNP particle and per particle surface area for different sizes of confeito-AuNPs. The data are represented as means ± SD, (n = 50).

Sample	Number of Tips/Particle	Number of Tips/Particle Surface Area (nm^2)
Confeito-AuNP 30 nm	23.7 ± 4.8	8.2×10^{-3}
Confeito-AuNP 60 nm	33.9 ± 3.2	2.8×10^{-3}
Confeito-AuNP 80 nm	52.2 ± 6.4	2.4×10^{-3}
Confeito-AuNP 100 nm	75.0 ± 9.5	1.1×10^{-3}

Unlike in serum-free DMEM, confeito-AuNPs suspended in complete culture media (DMEM supplemented with 10% FBS) presented hydrodynamic sizes comparable to those in water with a slight increase of approximately 10 nm (Table 1). This slight increase is most likely a result of the adsorption of plasma proteins from FBS onto the surface of confeito-AuNPs producing a multi-layered protein corona [25]. Because this protein corona on confeito-AuNPs is thin, it is unlikely to have a great impact on the cellular uptake and decreased targeting specificity [26].

The particle surface charges of all four confeito-AuNPs were approximately −11 mV when suspended in complete DMEM. This value was less negative than that in water (−34 to −43 mV) and even that in serum-free DMEM (−14 to −20 mV), probably because the corona formed by the adsorbed protein molecules shields the surface charge [27]. This interpretation concurs with the findings reported by Peuschel et al. [28] and Lesniak et al. [29] that NPs in complete cell culture medium have lower zeta potentials than those in serum-free media. Our results suggest that our confeito-AuNPs are favorable biomedical nanoparticles because it has been reported that nanoparticles with low surface charges (−15 mV) are more likely to evade phagocytosis by macrophages and to be internalized by non-phagocytic cells than nanoparticles with high negative charges [30]. According to Yamamoto et al.[31], low negative surface charges will also enhance the cell selectivity of nanoparticles and prevent non-specific binding to non-target cells before arriving at the target tumor site.

The tips of confeito-AuNPs (ends of bosses on spherical core surface) were evident (Fig. 1A and B). The total numbers of tips on the surfaces of confeito-AuNPs were estimated from FESEM images based on the mean of 50 particles and were divided by the surface area of the particles to normalize for the comparison of different sizes of confeito-AuNPs (Table 2). Although the largest size of confeito-AuNPs (100 nm) produced the highest total number

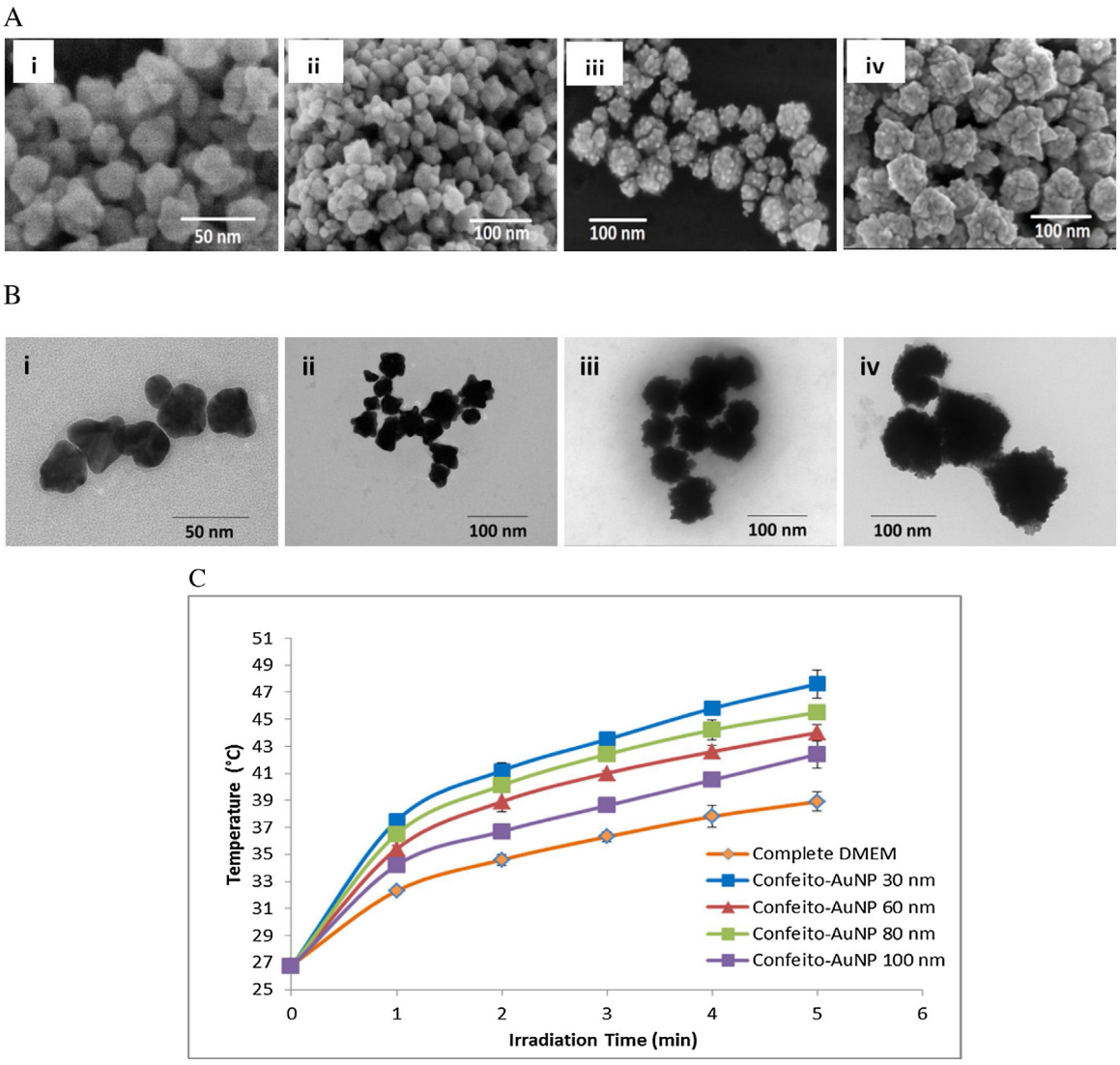

Fig. 1. Characterizations of confeito-AuNPs. (A) FESEM images of confeito-AuNPs at (i) 30 nm, (ii) 60 nm, (iii) 80 nm, and (iv) 100 nm. (B) TEM images of confeito-AuNPs at (i) 30 nm, (ii) 60 nm, (iii) 80 nm, and (iv) 100 nm. (C) Transient bulk temperature profiles of confeito-AuNP dispersions in complete DMEM under laser irradiation (2 W/cm^2, 5 min of irradiation). The data are represented as means ± standard deviation (SD), (n = 3).

of tips per particle (75 tips/particle), followed by a decrease in the total number of tips with the decreasing size of confeito-AuNPs, the smallest confeito-AuNPs (30 nm) produced the highest number of tips per unit particle surface area (8.2×10^{-3} tips/nm^2). The large number of tips per unit particle surface area corresponds to the dense or close existence of tips on AuNPs, indicating the increased plasmonic effect and intra- and inter-hot spot effect by confeito-AuNPs [32,33]. Thus, these effects may cause a strong photothermal therapeutic effect, which will be discussed later.

The bulk temperatures of suspensions of all four sizes of confeito-AuNPs were measured using a thermocouple. Under CW laser irradiation (2 W/cm^2), the bulk temperatures of all four sizes of confeito-AuNPs began to increase steadily from ambient room temperature (26.7 °C) (Fig. 1C) and reached ≈50% (7.5–10.8 °C increase) of the temperature increase at 5 min irradiation within the first one minute of irradiation. The rates of the temperature increase slowed down after the first one minute. It can be noted that all four sizes of confeito-AuNPs exhibited a higher bulk temperature increase than that of the control (complete DMEM without confeito-AuNPs), indicating that, upon laser irradiation, heat was produced via transfer from confeito-AuNPs to its surrounding through light energy harvest and conversion to heat energy in confeito-like AuNPs, resulting in a higher increase in the temperature of the medium by 10–20 °C.

Although this study employed a conventional method to investigate the bulk temperature increase of confeito-AuNPs, it was challenging to compare the thermal data directly with other published studies due to differences in the concentration and physical characteristics (shape and size) of NPs, as well as differences in the types and power intensity of the laser used for irradiation. In our study, the smallest size of confeito-AuNPs (30 nm) produced the highest temperature increase (21.3 ± 1.0 °C), while the largest size of confeito-AuNPs (100 nm) had the lowest temperature increase (16.1 ± 0.8 °C) than the other sizes (Fig. 1). On the other hand, confeito-AuNPs of 80 nm exhibited a slightly higher temperature elevation (18.5 ± 0.4 °C) than confeito-AuNPs of 60 nm (17.5 ± 0.3 °C). The results were largely in agreement with those of a previous study [34] that reported that the smallest AuNP of 31 nm had a higher photothermal conversion efficiency than other sizes of AuNP (47, 59, 74 and 86 nm). A smaller size of NP tends to have better photon to heat conversion efficiency relative to the larger size according to Mie's theory [35]. Although a bulk temperature increase of ≈ 10 °C was recorded for complete DMEM (control) during laser irradiation for 5 min (Fig. 1C), this is consistent with

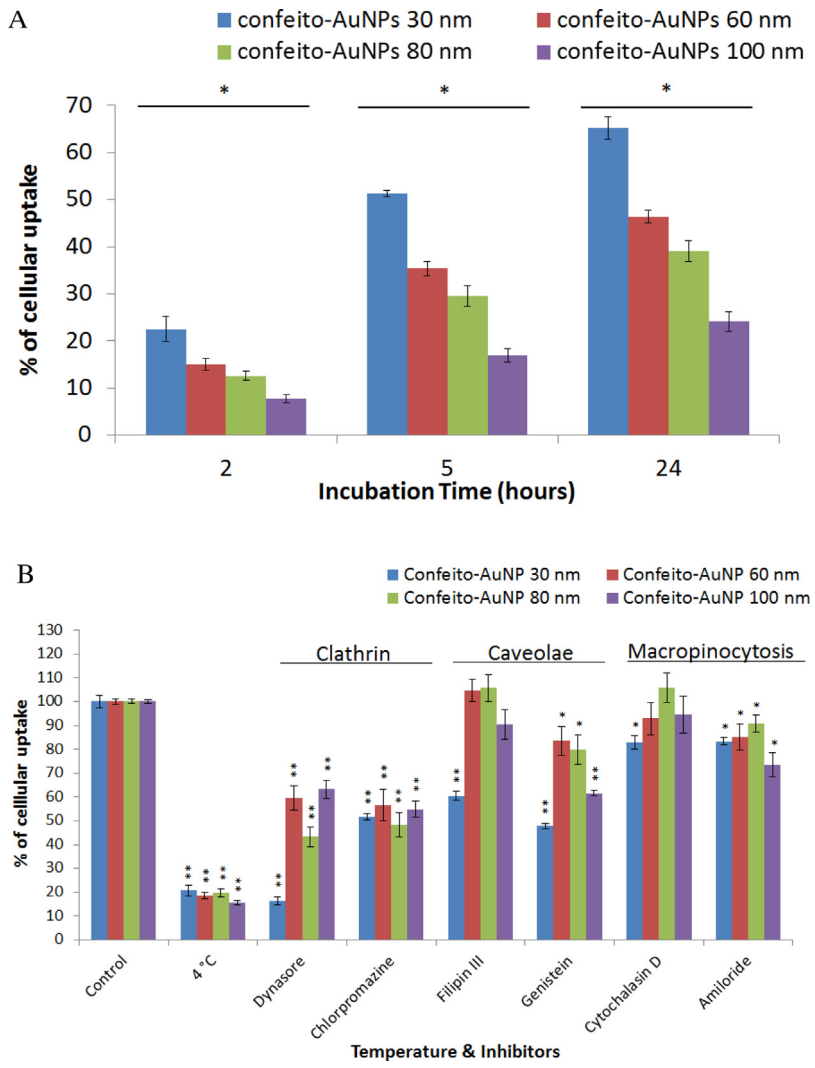

Fig. 2. Cellular uptake profile of confeito-AuNPs into MDA-MB-231 cells. (A) Confeito-AuNP uptake after 2 h, 5 h and 24 h of incubation. *$p < 0.05$ (ANOVA). (B) Energy-dependent cellular internalization of confeito-AuNPs and effect of transport inhibitors. *$p < 0.05$ and **$p < 0.01$ (independent T test) compared with the normalized control. The data are represented as means ± SD, (n = 3).

the observations reported by Liu et al. [36], where the temperature of water was increased by ≈ 7 °C under 980 nm laser irradiation (0.8 W/cm^2, 5 min) and that by Wong et al. [37], where an increase of ≈ 5 °C in water was observed under 520 nm light irradiation (0.5 W/cm^2, 5 min).

In addition to the effect of particle size, the effect of the plasmon phenomenon of AuNPs should be considered for their photothermal conversion efficiency. One of the motive forces of such a strong enhancement effect is the existence of edge or tips on NPs, where plasmon waves can be concentrated to provide hot spots. The distance and number of tips of bosses on the spherical core surface in confeito-AuNPs play an important role in heat production. It is reasonable that confeito-AuNPs of 30 nm with the highest number of tips per unit surface area generates more heat than those (60, 80 and 100 nm) with fewer tips per unit surface area. The results of this study agree with previous reports that the plasmon enhancement of confeito-AuNPs is associated with the number of tips on the surface of NPs. Additionally, the number of hot spots is also a contributory factor [33].

3.2. Cellular uptake of confeito-AuNPs

MP-AES was chosen to obtain the precise quantification of the amount of gold that has been taken up by cells. In the present study, cellular uptake was size and time dependent. The smallest size of confeito-AuNPs was indicative of the best cellular uptake into MDA-MB-231 cells compared with other sizes of confeito-AuNPs (Fig. 2A). A decreasing cellular uptake trend was observed for all incubation periods (2, 5 and 24 h) with an increasing size of confeito-AuNPs, and the uptake was always higher at the longer uptake time as expected.

The two smaller sizes of confeito-AuNPs (30 and 60 nm) produced better cellular internalization in agreement with the optimum size reported by others for cellular uptake (30–60 nm) [8,38,39]. Smaller nanoparticles with a diameter <25 nm were often detached from receptors easily due to the low binding affinity and failure to generate sufficient free energy for membrane wrapping [8,9], while nanoparticles >80 nm would require prolonged wrapping periods, causing lower cellular uptake [40]. Both extremely small and large nanoparticles would yield inefficient cellular uptake.

Although the size of confeito-AuNPs can be controlled during the synthesis process, the issue of protein adsorption onto the surface of confeito-AuNPs in complete cell culture medium must be considered in cellular uptake studies. Protein corona formation will lead to an increase in the hydrodynamic radius of confeito-AuNPs and, hence, affect the interactions with cells. It is important to determine the actual hydrodynamic size and whether confeito-AuNPs retain

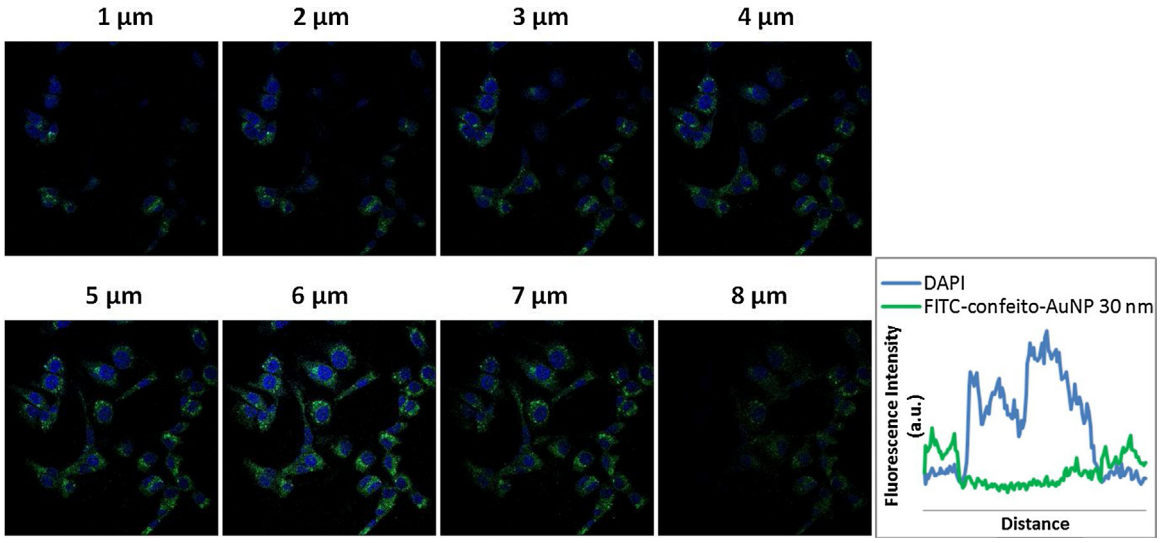

Fig. 3. Z-stack confocal microscopic images of MDA-MB-231 cells incubated for 5 h with FITC-confeito-AuNPs 30 nm and DAPI. The scale bars correspond to 20 µm.

their singularity in the biological media prior to cell entry. In addition, Cheng et al. [13] reported a size-dependent serum inhibition effect on the cellular uptake of confeito-AuNPs. With an increasing NP size, the inhibition effect of serum on the uptake of nanoparticles became greater. This may explain the lower cellular uptake with the increasing size of confeito-AuNPs.

3.2.1. Temperature effect and trafficking

Cellular uptake at 4 °C was reduced by approximately 80% for all four sizes of confeito-AuNPs relative to the uptake at 37 °C when incubated with MDA-MB-231 cells (Fig. 2B) ($p < 0.01$, independent T test). This suggests that the cellular internalization of confeito-AuNPs is energy dependent and probably occurs via endocytic pathways [41].

To determine the predominant endocytic pathway such as the clathrin-mediated pathway, caveolae-mediated endocytosis or macropinocytosis, and inhibitors such as chlorpromazine, dynasore, genistein, filipin III, cytochalasin D and amiloride, were used. The cytotoxicity of inhibitors against MDA-MB-231 cells was screened using the MTT assay prior to cellular uptake mechanism experiments. The cell viability of MDA-MB-231 incubated with selected concentrations of different inhibitors for 24 h was more than 90%, suggesting negligible toxicity from inhibitors (data not shown).

The uptake of 30-nm confeito-AuNPs was significantly inhibited by both dynasore (≈85%) and chlorpromazine (≈50%) relative to the control ($p < 0.01$, independent T test). Caveolae inhibitors Filipin III and genistein reduced the uptake of 30-nm confeito-AuNPs by ≈40% and ≈53%, respectively (Fig. 2B) ($p < 0.01$, independent T test). For the confeito-AuNPs of 60 nm, 80 nm and 100 nm, the uptake was predominantly inhibited by dynasore and chlorpromazine only. Macropinocytosis inhibitors (amiloride and cytochalasin D) did not significantly hinder the uptake of confeito-AuNPs for all four sizes. These results clearly suggest that the major internalization mechanisms for confeito-AuNPs of 30 nm were clathrin- and caveolae-mediated endocytosis, while the uptake of confeito-AuNPs of 60 nm, 80 nm and 100 nm occurred mainly via the clathrin-mediated pathway. The internalization of confeito-AuNPs of 30 nm by both clathrin and caveolae pathways probably explains its higher cellular uptake than other sizes of confeito-AuNPs.

Cheng et al. [13] reported a similar uptake mechanism (clathrin-mediated endocytosis) for 50 nm AuNP in Hep G2 cells and caveolae-mediated endocytosis for 20 nm AuNP. Thus, it is conceivable that nanoparticles of similar size can be internalized via different pathways in different cells. Additionally, the surface property and shape of NPs also have been indicated as important factors for the interaction between NPs and cells. Contrary to our findings where the cellular uptake of confeito-AuNPs of 30 nm was by a clathrin- and caveolae-mediated mechanism, Brandenberger et al. [42] reported that the uptake of similarly sized citrate-capped sphere-AuNPs into cells was by a macropinocytosis mechanism.

3.2.2. Intracellular localization of confeito-AuNPs

Intracellular localization of FITC-confeito-AuNPs (30, 60, 80 and 100 nm) in MDA-MB-231 cells was determined and analyzed using confocal microscopy. Images of cells treated with FITC-confeito-AuNPs co-stained with organelle-specific probes were captured, and localization topographic profiles were compared. As evidenced by the localization topographic profiles, minimal fluorescence overlaps between FITC-confeito-AuNPs and DAPI were shown (Fig. 3). This result suggests that even the smallest FITC-confeito-AuNPs (30 nm) were not localized in the nucleus after 5 h of incubation and is consistent with another report indicating that only nanoparticles with a size <5 nm could enter the cell nucleus [43].

Overall the fluorescence images and localization topographic profiles indicate that all four sizes of FITC-confeito-AuNPs were mainly localized in lysosomes and mitochondria instead of the endoplasmic reticulum after 2 h of incubation (Fig. 4A). The green fluorescence from all sizes of FITC-confeito-AuNPs overlapped with the blue fluorescence from LysoTracker and red fluorescence from Mitotracker as indicated in the topographic profiles. Other studies have shown that mitochondria provide the appropriate microenvironment for cysteine oxidation reactions [44], which may account for the localization of cystine/citric acid-coated confeito-AuNPs in this organelle. The localization of FITC-confeito-AuNPs in lysosomes is likely a result of their endocytic internalization into MDA-MB-231 cells, where lysosome is the last compartment of the endocytic pathway. Moreover, this finding is consistent with those in previous studies, indicating that clathrin-mediated endocytosis can direct gold nanomaterials to the endosomal/lysosomal compartment [45,46].

It was also noted that the smallest size of FITC-confeito-AuNPs (30 nm) produced higher localization in the endoplasmic reticulum than the other three sizes of confeito-AuNPs after 5 h of treatment (Fig. 4B). This result concurs with the caveolae-mediated endo-

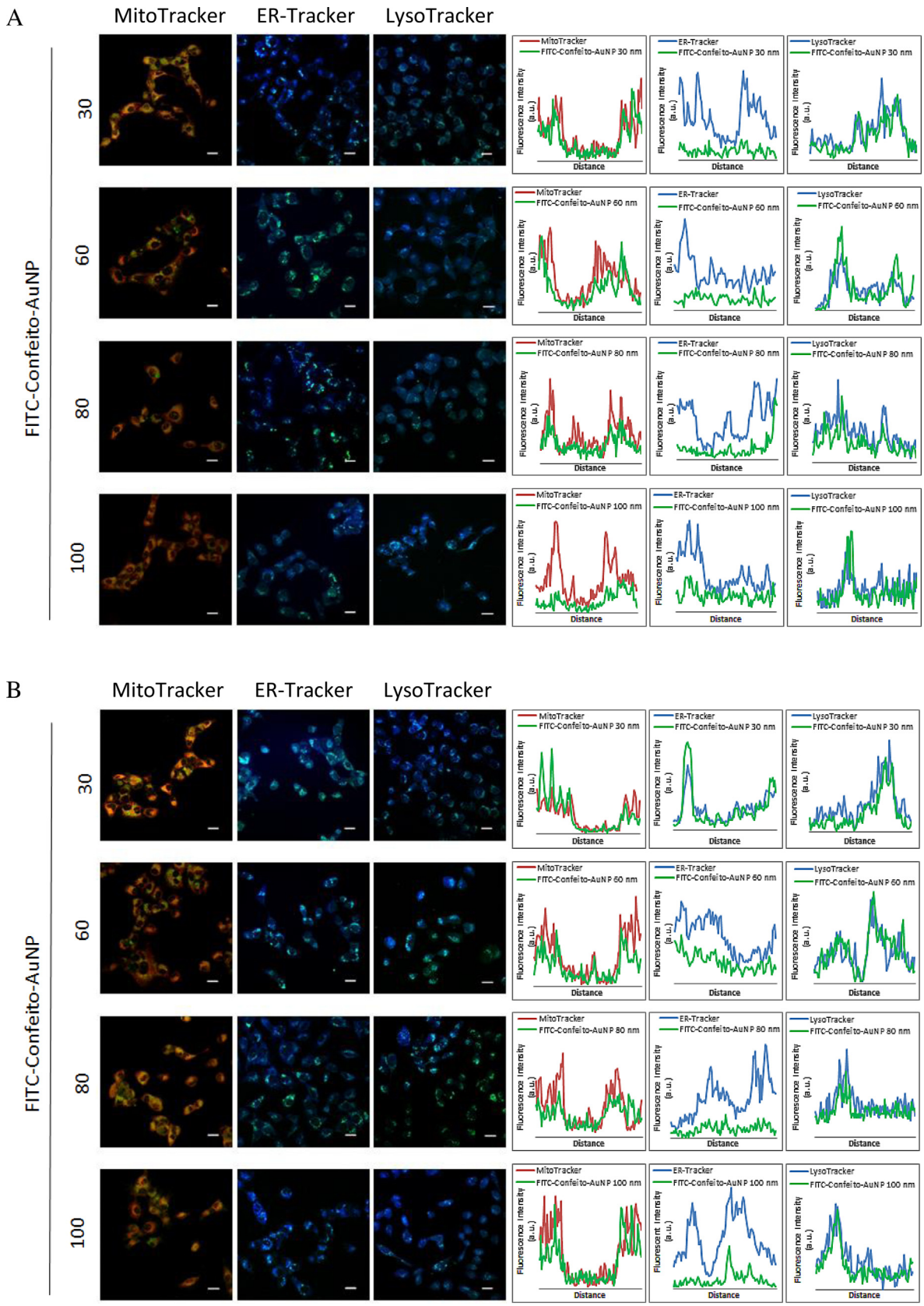

Fig. 4. Intracellular localization of FITC-confeito-AuNPs. (A) 2 h. (B) 5 h. The scale bars correspond to 20 μm.

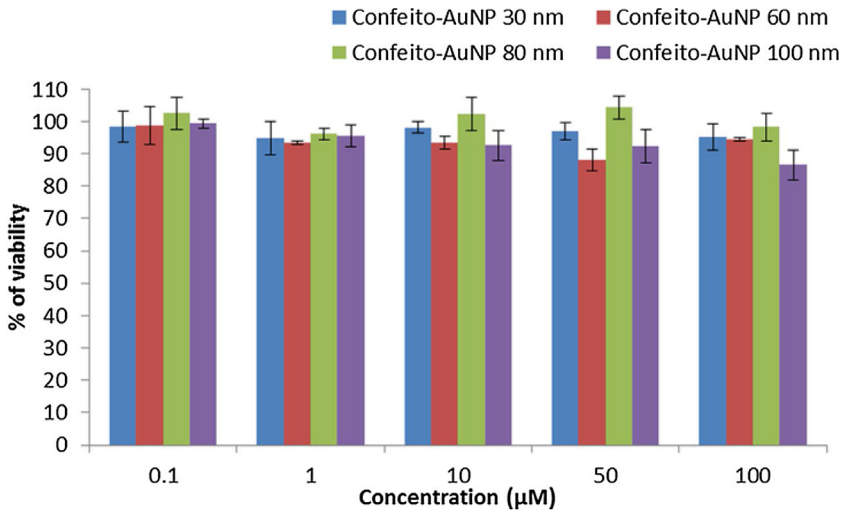

Fig. 5. MDA-MB-231 cell viability after incubation with confeito-AuNPs for 24 h without laser treatment. The data are represented as means ± SD, (n = 3).

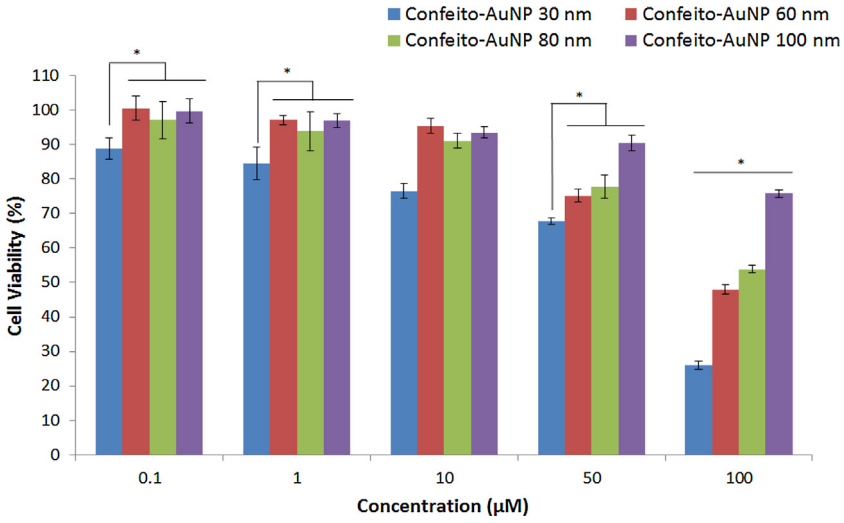

Fig. 6. *In vitro* photothermal treatment. (A) MDA-MB-231 cell viability post laser treatment (2 W/cm^2, 1 min of irradiation) by confeito-AuNPs. *p < 0.05 (ANOVA).

cytosis of confeito-AuNPs of 30 nm that can efficiently transport confeito-AuNPs to the perinuclear region such as the endoplasmic reticulum [46].

The intracellular localization of confeito-AuNPs was determined by stacking and analyzing 1-μm-thick slice images of MDA-MB-231 cell monolayer with cross-sectional slices perpendicular to the plane of the cell monolayer midpoint (z-axis) [23]. The presence of both fluorescence from DAPI (blue fluorescence) and FITC-confeito-AuNPs (green fluorescence) in the same slices (slice 4, 5, 6 and 7 μm) indicates that both cell nucleus and FITC-confeito-AuNPs are at the same depth (Fig. 3). These cross-sectional slices confirmed that FITC-confeito-AuNPs are located inside the cells.

3.3. In vitro *photothermal cancer therapy efficacy*

After 24 h of confeito-AuNP treatment, the MDA-MB-231 cancer cell viability was determined using the MTT assay (Fig. 5). Without laser irradiation, all four different sizes of confeito-AuNPs (30, 60, 80 and 100 nm) at 0.1–100 μM exhibited low toxicity with a cell viability of greater than 80% at 24 h of incubation.

After MDA-MB-231 cells were incubated with confeito-AuNPs for 2 h and were irradiated with a laser for only 1 min, a decrease in the cell viability for all four sizes of confeito-AuNPs was observed (Fig. 6). The smallest size (confeito-AuNPs 30 nm) displayed the highest photothermal cytotoxicity effect with a sharp decrease of ≈ 75% of cell viability, while the largest size of confeito-AuNPs (100 nm) displayed the lowest photothermal cytotoxicity effect with ≈ 15% cell death. The PTT effects of confeito-AuNPs demonstrate a trend that the cell killings decrease with increasing confeito-AuNPs size.

Based on Mie's theory that accounts for the interactions between particles and light scattering, Jain et al. [35] have reported that the photon absorption and scattering abilities are dependent on the size of the AuNP. A 20-nm AuNP can absorb almost the entire photon energy and convert it into heat energy. When the size increases to 40 nm, light scattering appears; when the size reaches 80 nm, the extinction is contributed equally by both absorption and scattering. Thus, the ratio of the scattering to absorption increases exponentially for larger sized particles. This might explain the smallest confeito-AuNPs (30 nm) producing the best performance in PTT treatment. Additionally, smaller NPs possess a high surface area relative to their total mass compared with larger NPs, enhancing NP-light interaction and triggering the photothermal anticancer effect.

The use of 532 nm laser with intensity set at 2 W/cm^2 has limited tissue penetration. Thus, we suggest using optical fibers as a light delivery medium to direct the light source and to ensure sufficient energy to activate gold nanoparticles for photothermal treatment of tumors located at a greater depth.

4. Conclusion

The present study provides a comprehensive understanding of the effect of NP characteristics on the cell-NP interaction. The size of confeito-AuNPs is the crucial factor affecting cellular uptake efficiency and photothermal anticancer treatment efficacy. We have shown that the smallest confeito-AuNPs (30 nm) have the highest MDA-MB-231 cellular internalization via two endocytic mechanisms: clathrin- and caveolae-mediated pathways. Other sizes of confeito-AuNPs enter the cells through only the clathrin-mediated pathway. The intracellular localization of confeito-AuNPs is related to the cellular uptake pathway, and it is evidenced that all the sizes of confeito-AuNPs are highly localized in the lysosome due to the clathrin-mediated pathway. Confeito-AuNPs (30 nm) have the highest localization in the endoplasmic reticulum compared with other sizes of confeito-AuNPs likely due to partial uptake via the caveolae-mediated pathway. In terms of photothermal treatment, confeito-AuNPs (30 nm) can increase the highest bulk temperature and display the highest photothermal cytotoxicity effect compared with other sizes of confeito-AuNPs. The present investigation indicates the potential of confeito-AuNPs as a PTT agent.

Acknowledgement

This bilateral collaborative project was supported by HIR-MoHE grants (UM.C/625/1/HIR/MOHE/MED/17 and UM.C/625/1/HIR/MOHE/MED/33) and UM postgraduate research grant (PG158-2015B). The authors would like to thank Hi-Tech Instruments for confocal service.

Appendix A. Supplementary data

Supplementary data associated with this article can be found, in the online version, at https://doi.org/10.1016/j.colsurfb.2017.10.064.

References

[1] J. Lee, D.K. Chatterjee, M.H. Lee, et al., Gold nanoparticles in breast cancer treatment: promise and potential pitfalls, Cancer Lett. 347 (1) (2014) 46–53.
[2] X. Huang, M.A. El-Sayed, Plasmonic photo-thermal therapy (PPTT), Alexandria J. Med. 47 (1) (2011) 1–9.
[3] X. Huang, I.H. El-Sayed, W. Qian, et al., Cancer cell imaging and photothermal therapy in the near-infrared region by using gold nanorods, J. Am. Chem. Soc. 128 (6) (2006) 2115–2120.
[4] Y. Liu, H. Yuan, A.M. Fales, et al., Multifunctional gold nanostars for molecular imaging and cancer therapy, Front. Chem. (2015) 3.
[5] F. Alexis, E. Pridgen, L.K. Molnar, et al., Factors affecting the clearance and biodistribution of polymeric nanoparticles, Mol. Pharm. 5 (4) (2008) 505–515.
[6] S. Prabha, W.-Z. Zhou, J. Panyam, et al., Size-dependency of nanoparticle-mediated gene transfection: studies with fractionated nanoparticles, Int. J. Pharm. 244 (1) (2002) 105–115.
[7] M.P. Desai, V. Labhasetwar, E. Walter, et al., The mechanism of uptake of biodegradable microparticles in Caco-2 cells is size dependent, Pharm. Res. 14 (11) (1997) 1568–1573.
[8] W. Jiang, B.Y. Kim, J.T. Rutka, et al., Nanoparticle-mediated cellular response is size-dependent, Nat. Nanotechnol. 3 (3) (2008) 145–150.
[9] S.-H. Wang, C.-W. Lee, A. Chiou, et al., Size-dependent endocytosis of gold nanoparticles studied by three-dimensional mapping of plasmonic scattering images, J. Nanobiotechnology 8 (1) (2010) 1.
[10] P. Liu, Y. Sun, Q. Wang, et al., Intracellular trafficking and cellular uptake mechanism of mPEG-PLGA-PLL and mPEG-PLGA-PLL-Gal nanoparticles for targeted delivery to hepatomas, Biomaterials 35 (2) (2014) 760–770.
[11] L. Shang, K. Nienhaus, G.U. Nienhaus, Engineered nanoparticles interacting with cells: size matters, J. Nanobiotechnology 12 (5) (2014) b26.
[12] N. Oh, J.-H. Park, Endocytosis and exocytosis of nanoparticles in mammalian cells, Int. J. Nanomed. 9 (Suppl 1) (2014) 51–63.
[13] X. Cheng, X. Tian, A. Wu, et al., Protein Corona influences cellular uptake of gold nanoparticles by phagocytic and nonphagocytic cells in a size-Dependent manner, ACS Appl. Mater. Interfaces 7 (37) (2015) 20568–20575.
[14] S. Mayor, R.E. Pagano, Pathways of clathrin-independent endocytosis, Nat. Rev. Mol. Cell Biol. 8 (8) (2007) 603–612.
[15] H.H. Richardson, M.T. Carlson, P.J. Tandler, et al., Experimental and theoretical studies of light-to-heat conversion and collective heating effects in metal nanoparticle solutions, Nano Lett. 9 (3) (2009) 1139–1146.
[16] J. Zeng, D. Goldfeld, Y. Xia, A plasmon-assisted optofluidic (PAOF) system for measuring the photothermal conversion efficiencies of gold nanostructures and controlling an electrical switch, Angew. Chem. Int. Ed. 52 (15) (2013) 4169–4173.
[17] C. Ayala-Orozco, C. Urban, M.W. Knight, et al., Au nanomatryoshkas as efficient near-infrared photothermal transducers for cancer treatment: benchmarking against nanoshells, ACS Nano 8 (6) (2014) 6372–6381.
[18] M. Ujihara, T. Imae, Versatile one-pot synthesis of confeito-like Au nanoparticles and their surface-enhanced Raman scattering effect, Colloids Surf. A: Physicochem. Eng. Asp. 436 (2013) 380–385.
[19] M. Longmire, P.L. Choyke, H. Kobayashi, Clearance Properties of Nano-Sized Particles and Molecules as Imaging Agents: Considerations and Caveats, 2008.
[20] S.D. Conner, S.L. Schmid, Regulated portals of entry into the cell, Nature 422 (6927) (2003) 37–44.
[21] J. Wan, J.-H. Wang, T. Liu, et al., Surface chemistry but not aspect ratio mediates the biological toxicity of gold nanorods in vitro and in vivo, Sci. Rep. 5 (2015) 11398.
[22] X. Gao, K. Stanger, H. Kaluarachchi, et al., Cellular uptake of a cystine-knot peptide and modulation of its intracellular trafficking, Sci. Rep. 6 (2016) 35179.
[23] G. Viswanathan, Y.H. Hsu, S.H. Voon, et al., A comparative study of cellular uptake and subcellular localization of doxorubicin loaded in self-assemblies of amphiphilic copolymers with pendant dendron by MDA-MB-231 human breast cancer cells, Macromol. Biosci. 16 (6) (2016) 882–895.
[24] S. Edwards, D. Williams, Double layers and interparticle forces in colloid science and biology: analytic results for the effect of ionic dispersion forces, Phys. Rev. Lett. 92 (24) (2004) 248303.
[25] C.D. Walkey, J.B. Olsen, H. Guo, et al., Nanoparticle size and surface chemistry determine serum protein adsorption and macrophage uptake, J. Am. Chem. Soc. 134 (4) (2012) 2139–2147.
[26] J.C.Y. Kah, C. Grabinski, E. Untener, et al., Protein coronas on gold nanorods passivated with amphiphilic ligands affect cytotoxicity and cellular response to penicillin/streptomycin, ACS Nano 8 (5) (2014) 4608–4620.
[27] A.C. Sabuncu, J. Grubbs, S. Qian, et al., Probing nanoparticle interactions in cell culture media, Colloids Surf. B: Biointerfaces 95 (2012) 96–102.
[28] H. Peuschel, T. Ruckelshausen, C. Cavelius, et al., Quantification of internalized silica nanoparticles via STED microscopy, BioMed Res. Int. (2015) 2015.
[29] A. Lesniak, F. Fenaroli, M.P. Monopoli, et al., Effects of the presence or absence of a protein corona on silica nanoparticle uptake and impact on cells, ACS Nano 6 (7) (2012) 5845–5857.
[30] S.H. Voon, S.X. Tiew, C.S. Kue, et al., Chitosan-coated poly (lactic-co-glycolic acid)-diiodinated boron-dipyrromethene nanoparticles improve tumor selectivity and stealth properties in photodynamic cancer therapy, J. Biomed. Nanotechnol. 12 (7) (2016) 1431–1452.
[31] Y. Yamamoto, Y. Nagasaki, Y. Kato, et al., Long-circulating poly (ethylene glycol)-poly (d, l-lactide) block copolymer micelles with modulated surface charge, J. Controlled Release 77 (1) (2001) 27–38.
[32] M. Ujihara, N.M. Dang, C.-C. Chang, et al., Surface-enhanced infrared absorption spectra of eicosanoic acid on confeito-like Au nanoparticle, J. Taiwan Inst. Chem. Eng. 45 (6) (2014) 3085–3089.
[33] C.-C. Chang, T. Imae, L.-Y. Chen, et al., Efficient surface enhanced Raman scattering on confeito-like gold nanoparticle-adsorbed self-assembled monolayers, Phys. Chem. Chem. Phys. 17 (48) (2015) 32328–32334.
[34] M.-J. Chiu, L.-K. Chu, Quantifying the photothermal efficiency of gold nanoparticles using tryptophan as an in situ fluorescent thermometer, Phys. Chem. Chem. Phys. 17 (26) (2015) 17090–170100.
[35] P.K. Jain, K.S. Lee, I.H. El-Sayed, et al., Calculated absorption and scattering properties of gold nanoparticles of different size, shape, and composition: applications in biological imaging and biomedicine, J. Phys. Chem. B 110 (14) (2006) 7238–7248.
[36] Y. Liu, J.R. Ashton, E.J. Moding, et al., A plasmonic gold nanostar theranostic probe for in vivo tumor imaging and photothermal therapy, Theranostics 5 (9) (2015) 946–960.
[37] Temperature measurements of a gold nanosphere solution in response to light-Induced hyperthermia, In: J.K. Wong, R. Taylor, S. Baek, et al., ASME 2013 International Mechanical Engineering Congress and Exposition, American Society of Mechanical Engineers (2013).
[38] B.D. Chithrani, A.A. Ghazani, W.C. Chan, Determining the size and shape dependence of gold nanoparticle uptake into mammalian cells, Nano Lett. 6 (4) (2006) 662–668.
[39] A. Malugin, H. Ghandehari, Cellular uptake and toxicity of gold nanoparticles in prostate cancer cells: a comparative study of rods and spheres, J. Appl. Toxicol. 30 (3) (2010) 212–217.
[40] H. Gao, W. Shi, L.B. Freund, Mechanics of receptor-mediated endocytosis, Proc. Natl. Acad. Sci. 102 (27) (2005) 9469–9474.

[41] S. Hong, R. Rattan, I.J. Majoros, et al., The role of ganglioside GM1 in cellular internalization mechanisms of poly (amidoamine) dendrimers, Bioconjugate Chem. 20 (8) (2009) 1503–1513.
[42] C. Brandenberger, C. Mühlfeld, Z. Ali, et al., Quantitative evaluation of cellular uptake and trafficking of plain and polyethylene glycol-coated gold nanoparticles, Small 6 (15) (2010) 1669–1678.
[43] K. Huang, H. Ma, J. Liu, et al., Size-dependent localization and penetration of ultrasmall gold nanoparticles in cancer cells, multicellular spheroids, and tumors in vivo, ACS Nano 6 (5) (2012) 4483–4493.
[44] R.J. Mailloux, X. Jin, W.G. Willmore, Redox regulation of mitochondrial function with emphasis on cysteine oxidation reactions, Redox Biol. 2 (2014) 123–139.
[45] A. Chakraborty, N.R. Jana, Clathrin to lipid raft-endocytosis via controlled surface chemistry and efficient perinuclear targeting of nanoparticle, J. Phys. Chem Lett. 6 (18) (2015) 3688–3697.
[46] J. Rejman, A. Bragonzi, M. Conese, Role of clathrin-and caveolae-mediated endocytosis in gene transfer mediated by lipo-and polyplexes, Mol. Ther. 12 (3) (2005) 468–474.